

ENCODING OF TOPOLOGICAL INFORMATION IN MULTI-SCALE REMOTELY SENSED DATA: APPLICATIONS TO SEGMENTATION AND OBJECT-BASED IMAGE ANALYSIS

Abdul Haleem Syed^{a,*}, Eli Saber^{a,b}, and David Messinger^a

^a Chester F. Carlson Center for Imaging Science, Rochester Institute of Technology,
Rochester, New York, USA 14623 - has1061@rit.edu*, messinger@cis.rit.edu

^b Department of Electrical and Microelectronic Engineering, Rochester Institute of Technology,
Rochester, New York, USA 14623 - essee@rit.edu

KEY WORDS: Spatial Processing, Topology, 9-Intersection model, RCC-8, Combinatorial Maps, Scale-tree, Objected-based Image Analysis, Multi-scale Segmentation

ABSTRACT:

With rapid developments in satellite and sensor technologies, there has been a dramatic increase in the availability of high resolution (HR) remotely sensed images ($< 1m$). There is a growing need for automated image analysis techniques which go beyond the traditional pixel based methods. Novel methods are needed that leverage the abundant spatial, contextual, and topological information now available in HR images. Mapping of a region in an image, into a meaningful object, requires analyzing not only features such as the spectral signature, texture, and shape but also examining its topology. The ability to leverage contextual information requires examining a regions (potential object's) neighborhood, and examining the arrangement of adjacent regions. In this paper, we compare two different methods to model and encode the topology of regions namely the Region Connection Calculus (RCC-8 model) and the Combinatorial Maps model (CM). We demonstrate that the RCC-8 topological predicates can be elegantly derived using the CM model. A procedure to query the topology of regions using the CM models is presented. A performance comparison between the pixel-based (RCC-8) v.s. dart-based (CM model) topological queries indicates that the CM model is much more efficient and provides a better framework for topological analysis.

1 INTRODUCTION

The new WorldView-2 Sensor can capture images with spatial resolution less than $0.5m$ (Pan Chromatic) and can cover the entire area of U.S.A. in 12 days. Such recent improvements in satellite technology have dramatically increased our collection capacity, dictating a need for methods/techniques of image analysis that can automatically extract meaningful information from these images.

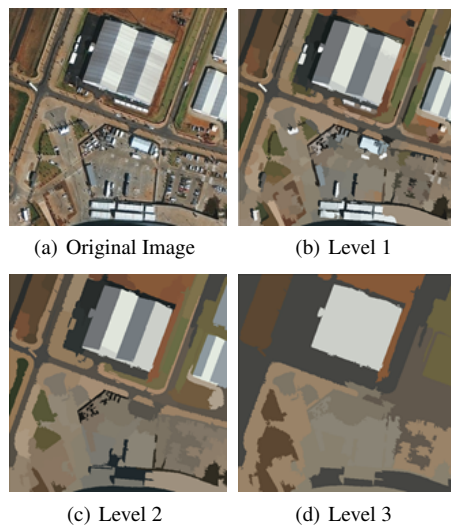


Figure 1: Objects appear as coherent image regions at different levels. The biggest object in image(a) is over-segmented in levels 1 & 2 but appears as a coherent region in level 3.

Segmentation is a common pre-processing step in image analysis where pixels are grouped into homogeneous image regions based on some criteria. Segmentation of high-resolution remotely

sensed images poses unique challenges such as the issue of scale. A single segmentation is not adequate to describe a complex high resolution image, as the objects of interest may appear at different scales with no prior information on what those scales are (see Figure 1). This has led to a surge in multi-scale-segmentation techniques in the literature, as described in a survey paper on segmentation with a remote sensing perspective (Dey et al., 2010).

These multi-scale representations are hierarchical in nature and are derived through various groupings of image pixels/regions which are homogeneous in the feature space. Commonly used features are spectral signature, texture and shape. Mapping of a region in an image into a meaningful object requires analyzing, not only the traditional features but also examining its topology. Examining an object's relationship to the adjacent regions and the arrangement of its sub-parts provides additional information that is not captured in the usual geometric and radiometric properties. Methods and techniques that can efficiently query topological relationships are needed. Such methods would also support one of the goals of Geographic Object Based Image Analysis (GEOBIA) to develop the ability to query and link individual objects (a.k.a segments) in space and time (Hay and Castilla, 2006).

To facilitate image analysis of complex images a multi-scale representation called the Scale-Space Representation was proposed in (Syed et al., 2011). This representation which is based on the principles of object oriented design, the scale-tree, contains the scale-space of the image storing inside it segmentations of varying levels of detail. Each level differs from the next in the size of the objects that it represents. A scale-tree of an image is shown in Figure 2. Each node of the tree represents a region in the image. The tree was built bottom up based on the spectral signature of the region. In addition to the low level descriptors such as spectral and geometric, our goal is to add on topological descriptors for each node/region.

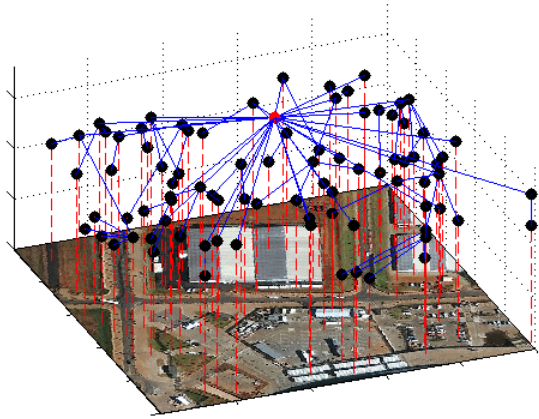


Figure 2: Scale-Tree for the image shown in Figure 1(a). Each region is displayed as a node. The position of the node on the vertical axis is a function of its position in the scale-space. Tree captures the relationships between regions of different levels of a multi-scale segmentation.

In this paper, we look at two different models that extract and encode the topology of image regions and their application to remotely sensed images. Section 2 describes a popular method used to model the topology of regions called the Region Connection Calculus (RCC-8 model). The RCC-8 model was successfully adapted by (Inglada and Michel, 2007) to perform object search. The authors used a template image and a topologically encoded multi-scale segmentation to detect airplanes in a high resolution image. Section 3 describes the Combinatorial Maps (CM) model to encode and query the topology of image regions. Section 4 presents preliminary results where RCC-8 predicates are derived using the CM model and a topologically encoded segmentation of an image from the WorldView-2 sensor is presented. Finally, conclusions are drawn in Section 5.

2 THE REGION CONNECTION CALCULUS (THE RCC-8 MODEL)

In this section, a brief introduction of the RCC-8 Model is provided followed by a discussion of how this model is applied to real images. See (Randell et al., 1992, Egenhofer, 1991) for a more detailed treatment of this model.

The Region Connection Calculus (RCC) by Randell, Cui, and Cohn (Randell et al., 1992) is a widely used formalism for qualitative spatial reasoning. The RCC-8 model provides a framework to determine the topological relationships between two simple regions. Given two regions A and B, eight unique configurations between two different regions are defined (see Figure 3).

$$M = \begin{pmatrix} A^\circ \cap B^\circ & A^\circ \cap \partial B & A^\circ \cap B^- \\ \partial A \cap B^\circ & \partial A \cap \partial B & \partial A \cap B^- \\ A^- \cap B^\circ & A^- \cap \partial B & A^- \cap B^- \end{pmatrix} \quad (1)$$

Independently, Egenhofer (Egenhofer, 1991) developed the 9-intersection model in the area of geographic information systems (GIS) which leads to same set of topological predicates for two spatial regions. Assessing the topological relationship between the regions involves decomposing each region into its boundary (∂A), interior (A^-) and exterior (A°) and examining the intersections as shown in Equation 1.

One way to compute the elements needed for the 9-intersection matrix, of Equation (1), is presented in (Inglada and Michel,

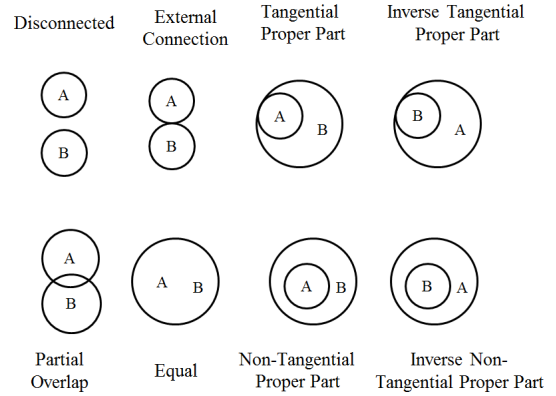


Figure 3: Eight possible topological configurations between two spatial regions A and B

2007). A binary mask representing the region is obtained from the segmentation step. A complement of the mask represents the exterior (A°) of the region, the interior (A^-) is obtained by morphological erosion using a structuring element of size 1pixel. Finally, the boundary (∂A) is obtained by taking a difference of interior from the mask (see Figure 4). This process is repeated for the second region to obtain B° , B^- and ∂B . Finally, the intersections to be used in the matrix can be computed by an addition of the binary masks.

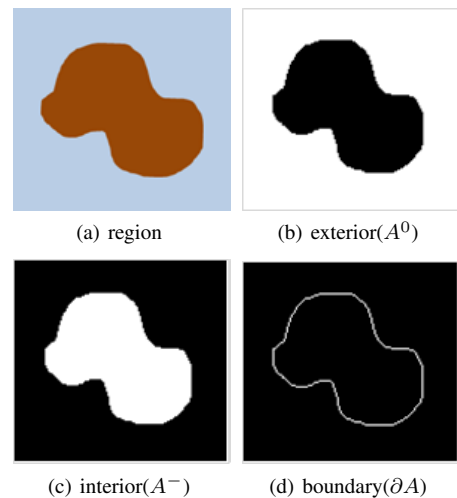


Figure 4: Illustration of a regions boundary, exterior, and interior obtained from a binary mask of the region. Note that the three elements A° , A^- , and ∂A are all defined on pixels.

As the number of regions of a segmentation increases, so does the computation time required to extract the exterior, interior, and the boundary. A better way to compute the elements needed to derive the RCC8 relationships is to use a vector representation of the boundary of regions (Inglada and Michel, 2009). In order to handle complex regions, such as those found in real images, a number of extensions of RCC-8 model have been proposed (Alboody et al., 2009, Behr and Schneider, 2001) but the extraction and encoding approach remain the same. Querying the topological relationship between a new arrangement, of two regions, requires computation of the M matrix shown in Equation (1) and comparison to the eight configurations shown in Figure 3.

3 THE COMBINATORIAL MAPS MODEL (CM MODEL)

In this section we present the combinatorial maps model which encodes the topology of the 2D Euclidean space. We start with definitions and proceed to show how this formalism can be applied to images. See (Braquelaire, 2005, Damiani et al., 2004, Braquelaire and Domenger, 1999) for a more detailed explanation of the underlying concepts.

3.1 The CM Model Definitions

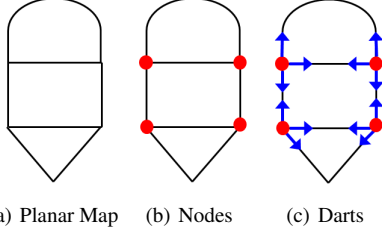


Figure 5: Subdivision of the Euclidean space.

A partition of the Euclidean plane into simply connected regions is called a **Planar Map**. A planar map can be broken down into simpler elements called nodes, edges and faces. A **node** is a point of intersection of three or more edges, the red disks in Figure 5(b). An **edge** is defined a connection between two nodes. Each edge is further subdivided into two darts, shown as blue arrows in Figure 5(c). Each **dart** “ d ” defines a segment which is an oriented edge. This addition of orientation allows us to separate the direction in which we traverse an edge. Darts belonging to the same edge are encoded with “ $+d$ ” and “ $-d$ ”. A sample labeling is shown in Figure 6(a).

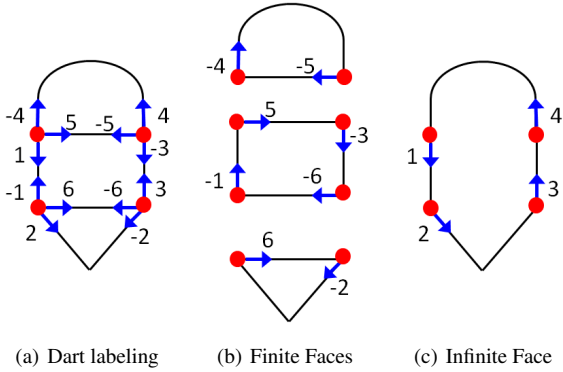


Figure 6: Dart labeling to define segments. Finite and infinite faces are defined by the direction in which the segments are traversed.

A **face** is a simply connected region contained inside a closed curve. A finite face is defined by a clockwise traverse of the segments as shown in Figure 6(b) and an infinite face is defined when the segments are traversed in the counter-clockwise direction, see Figure 6(c).

A **combinatorial map** G is the triplet $G = (D, \sigma, \alpha)$, where D is the set of darts σ and α , are two permutations defined on D such that $\alpha(d) = -d$. The cycle of the permutation σ denoted by σ^* encodes the nodes as shown in Figure 7.

A cycle of a permutation σ^* defines the vertex. For example, vertex 1 is defined by the counter-clockwise cycle $\sigma^* = (-4, 1, 5)$ and vertex 2 is defined by $\sigma^* = (-5, -3, 4)$. Each entry of σ encodes the next dart that is met when turning counter-clockwise

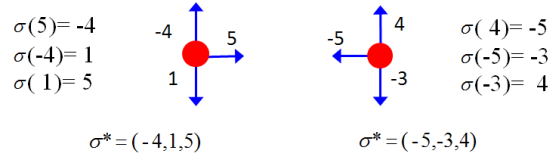


Figure 7: Deriving the permutation σ

around the vertex (see Figure 7). Once all the cycles of sigma are known, the permutation can be encoded in a linear array, indexed by darts as shown in Table 1, which has all the information to reconstruct the topology of Figure 6(a). The permutation α is implicitly encoded therefore it need not be saved.

d	1	-1	2	-2	3	-3	4	-4	5	-5	6	-6
σ	5	2	6	3	-6	4	-5	1	-4	-3	-1	-2

Table 1: σ encoded as an array of integers indexed by darts.

Finally, the cycles of permutation φ encode the face, which is defined as $\varphi = \alpha \circ \sigma$. Where \circ denotes composition of functions σ and α . A cycle of φ gives the set of darts encountered when traversing the face. This permutation defines the dual of our primal graph as $\bar{G} = (D, \varphi, \alpha)$. Computation of for a simple face from Figure 6(a) is shown in Figure 8 below. Once the darts of a face are identified, they can be assigned the same label for efficient access and retrieval.

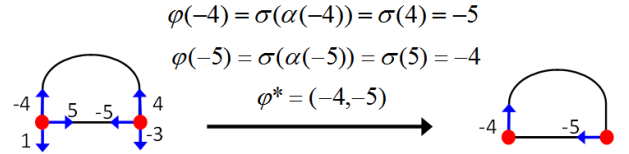


Figure 8: Deriving the permutation φ for a finite face from Figure 6(a).

3.2 Applying the CM Model to Image Regions

Application of the CM model to real images starts with the Label Map (Figure 9(b)) which can be generated through an initial segmentation of choice. The Label Map should have unique labels for each region. The labeled region map is then scanned to find all the boundaries and node points (Figure 9(c)). The boundary map is stored and saved in an array called boundary image, **BI** of size $(M + 1) \times (N + 1)$ where the original image is $M \times N$. The BI encodes the interpixel boundary of the image (Braquelaire and Brun, 1998).

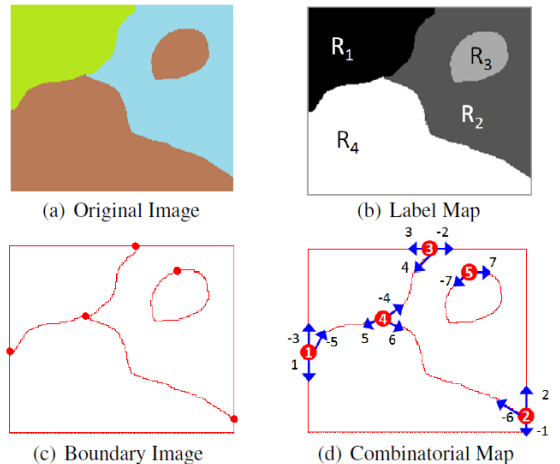


Figure 9: Deriving the Combinatorial Map of the image.

Once the **node** points have been identified, the red circles Figure 9(c), each boundary segment is labeled with the darts. *One end* of the segment is encoded by a positive integer “+ d ” and the *other end* of the same segment is encoded with “- d ” as shown in Figure 9(d). Using the procedure described in Section 3.1 the array σ is built. For easy access to regions all darts belonging to a region are given the same label which is stored in an array called λ .

d	σ	λ	d	σ	λ	<i>region</i>	<i>father</i>
1	-5	0	-4	5	2	1	0
-1	2	4	5	6	1	2	0
2	-6	0	-5	-3	4	3	2
-2	3	2	6	-4	4	4	0
3	4	0	-6	-1	2		
-3	1	1	7	-7	5		
4	-2	1	-7	7	3		

Table 2: Topology of regions from Figure 9(b) encoded as arrays of integers.

Combinatorial maps represent the topology of the Euclidean space defined by connected boundary components. The boundary of region R_3 is not connected to the rest of the boundary; therefore it will be defined by its own combinatorial map. To capture the relationship of the R_3 to R_2 , an array *father* is initialized and maintained during the construction. The father array serves a similar purpose as an *inclusion tree* (Damiand et al., 2004) giving a complete the combinatorial map representation.

Once the combinatorial representation has been built, each region can now be addressed by a set of darts which define its outer boundary. Recall from Section 3.1 that a finite face (image region) is encoded by a set of darts encountered when traversing its boundary in a clockwise direction. That is, the regions are now identified by darts representing the segments of their boundary. Applying this to the Figure 9(d), we have : $R_1 = (-3, 4, 5)$, $R_2 = (-2, -6, 4)$, $R_3 = (-7)$, and $R_4 = (-1, -5, 6)$.

3.3 Querying Topological Adjacency & Containment

Checking for the topological relationships is now reduced to looking at the darts, that define the regions, stored in array σ and the inclusion relationships which are captured by the array *father*. Querying for adjacency relationship can be done in the following fashion. Let R_i and R_j be two regions in an image. Then the regions R_i and R_j are adjacent if and only if

$$-d_i = d_j \quad (2)$$

where $d_i \in R_i$ and $d_j \in R_j$. Note that this will only be true when the two regions share a common edge. Consider checking for adjacency between R_1 and R_4 of Figure 9(b). The regions share a common edge which appears as dart 5 in R_1 and dart -5 in R_4 , therefore they are adjacent. On the other hand querying for containment relationships between regions is done by looking at the array *father*. Please note that we use the ‘ \subset ’ symbol to signify a containment relationship between two regions. Does the region R_j contain the region R_i ? Formally, this can be answered as, $R_i \subset R_j$ if and only if

$$father(R_i) = R_j \quad (3)$$

4 RESULTS AND DISCUSSION

In this section, we first present the results of our derivation of topological predicates of the RCC-8 Model using the CM model

(Section 4.2). A simple image(Figure10) and its CM representation will be used to illustrate the derivation. Section 4.3, outlines the process used to query the topology of any two regions using their dart representation. Finally, in Section 4.4 a simple performance comparison between, the topological queries using the, pixel-based representation and dart-based representations is performed. Finding the region-adjacency-list, which is a frequently required step in segmentation, will be used to perform the comparison.

4.1 Example Image and it’s Dart-based Representation

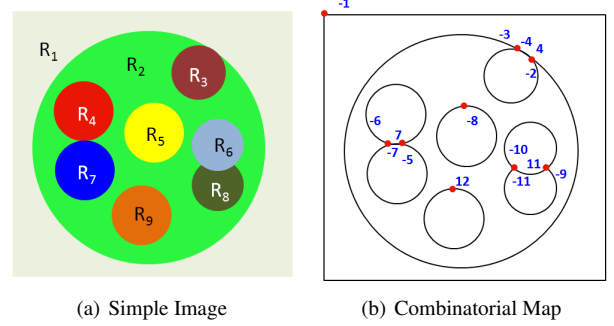


Figure 10: Simple image with regions in various topological arrangements. Note that in (b) only the darts representing the regions are shown to avoid clutter.

Consider the simple image (Figure 10) with multiple regions of various topological arrangements. A dart based representation of the image is generated using the the CM model as explained in Section 3. The results are presented in the Table 3.

d	σ	d	σ	<i>region</i>	<i>father</i>	<i>Region Darts</i>
1	-1	7	-5	1	0	$R_1 = (-1)$
-1	1	-7	-6	2	1	$R_2 = (4, -3)$
2	-4	8	-8	3	2	$R_3 = (-2, -4)$
-2	3	-8	8	4	2	$R_4 = (-6, 7)$
3	4	9	-11	5	2	$R_5 = (-8)$
-3	2	-9	10	6	2	$R_6 = (-10, 11)$
4	-2	10	11	7	2	$R_7 = (-5, -7)$
-4	-3	-10	9	8	2	$R_8 = (-9, -11)$
5	-7	11	-9	9	2	$R_9 = (-12)$
-5	6	-11	-10			
6	7	12	-12			
-6	5	-12	12			

Table 3: Topology of regions, from Figure 10(a), encoded as arrays of integers.

4.2 Deriving the RCC-8 Relationships Using The CM Model

Let R_i and R_j be two regions under consideration and let $d_i \in R_i$ and $d_j \in R_j$. Let us now take a look at RCC-8 topological arrangements.

Disconnected (DC) : Two regions will be disconnected if they do not contain each other and do not have no common darts. For example R_5 and R_9 in Figure 10(a) are DC. More formally the following condition needs to be satisfied:

$$R_i \not\subset R_j \ \& \ R_j \not\subset R_i \\ -d_i \notin R_j \ \& \ -d_j \notin R_i \quad (4)$$

External Connection (EC) : Two regions will be externally connected if they do not contain each other and share at least one

common edge. More formally :

$$\begin{aligned} R_i \not\subset R_j \ \& \ R_j \not\subset R_i \\ -d_i \in R_j \ \text{or} \ -d_j \in R_i \end{aligned} \quad (5)$$

Consider regions R_4 and R_7 from Figure 10(a). A closer view is provided in Figure 11 below. $R_4 = (-6, 7)$ and $R_7 = (-5, -7)$. Using Equation 3 to check containment we get $R_4 \not\subset R_7$, $R_7 \not\subset R_4$. From the region defining darts, we can see that $-7 \in R_7$ or $7 \in R_4$ therefore R_4 and R_7 are EC. Similarly, we can see that regions R_6 and R_8 are EC and regions R_2 and R_3 are not EC.

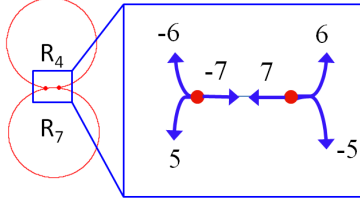


Figure 11: Closer examination of R_4 and R_7

Tangential Proper Part (TPP) or Inverse Tangential Proper Part (TPP^{-1}): Two regions will have a Tangential Proper Part relationship if one of the regions contains the other and they share a common edge. The order of the containment will decide whether the topology is TPP (Equation 6) or TPP^{-1} (Equation 7).

$$R_j \subset R_i, \ -d_i \in R_j \ \text{or} \ -d_j \in R_i \quad (6)$$

$$R_i \subset R_j, \ -d_i \in R_j \ \text{or} \ -d_j \in R_i \quad (7)$$

Consider regions $R_2 = (-3, 4)$ and $R_3 = (-2, -4)$ from Figure 10(a). Using the array *father* we see that $R_3 \subset R_2$ and $-4 \in R_3$, therefore, region R_3 is a TPP of region R_2 .

Non-Tangential Proper Part (NTPP) or Inverse Non-Tangential Proper Part ($NTPP^{-1}$): The regions will have a Non-Tangential Proper Part relationship if one of the regions fully includes the other and they do not share a common edge. Again, the order of the containment will decide whether the topology is NTPP (Equation 8) or $NTPP^{-1}$ (Equation 9).

$$R_j \subset R_i, \ -d_i \notin R_j \ \text{or} \ -d_j \notin R_i \quad (8)$$

$$R_i \subset R_j, \ -d_i \notin R_j \ \text{or} \ -d_j \notin R_i \quad (9)$$

In Figure 10(a), consider regions $R_2 = (-3, 4)$ and $R_5 = (-8)$. Using the array *father* we see that $R_5 \subset R_2$ and the regions do not share any darts. Therefore, R_5 is NTPP of R_2 .

Partial Overlap (PO) and Equivalence (EQ): Given the nadir view of remotely sensed images and the nature of the objects being imaged (opaque) the PO relationships appears as occlusion. Within our framework overlapping regions will appear as externally connected (EC) with some part of a region occluded by the other. Also, the Equivalence (EQ) relationship cannot be inferred from the nadir image as occlusion will only allow the top region to be visible.

4.3 Querying the topology of any two regions R_i and R_j

The nature of the RCC-8 relationship between two regions can be found quickly by using the dart representation. The procedure to do so is described in Figure 12. We zero in on the unique RCC-8 configuration by first checking if the regions share any common darts (indicating common boundary). We then proceed to check the containment relationships using the array *father*(.).

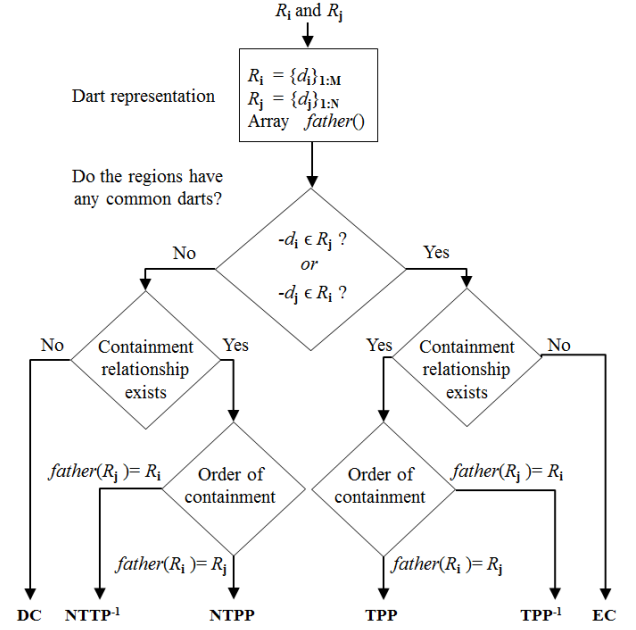


Figure 12: Flow chart to querying topological relationship between two regions using the dart representation

4.4 Performance Comparison

Finding all regions surrounding a specified region is a frequently required operation in image segmentation. For example, the Size-constrained-region-merging algorithm for segmentation of remotely sensed images uses a region-adjacency-list to aid the merging decision (Castilla et al., 2008). This step becomes a bottle neck when the images being segmented are large high-resolution images that need to be segmented at multiple levels.

Segmentation Level	# of Regions in Segmentation	Computation	Time (sec)
		pixel-based	dart-based
L3	4,050	2.82	0.46
L2	7,097	5.94	1.36
L1	8,537	7.69	1.84

Table 4: Comparing the time required to generate a region-adjacency-list for all the regions in an image for multiple segmentations.

A computation of the region-adjacency-list for all regions in a given image is performed by using both the pixel-based and the dart-based methods. Methods described in Section 2 are used for pixel-based computation of adjacency. While the CM model representation described in Section 3 is used to find the adjacencies for the pixel-based approach. The image used for the comparison is shown in Figure 13(a). This image is a small part of Al-Masirah island in Oman captured by the WorldView-2 Sensor with a spatial resolution $< 0.5m$ in GSD. The image was segmented to have a minimum region size (MRS) of 25, 75 and 125 pixels receptively as shown in Figure 13. The computation times, to compute the region-adjacency lists, using both the methods are shown in Table 4. The computations were performed on an Intel i7 CPU @2.8 GHz and 6GB RAM, using MATLAB R 2010a.

Please note that the computation of the region-adjacency list is being done for comparison purposes. Unlike the pixel-based methods, with the CM model, computing and updating the region-adjacency-list is not required. The CM model framework allows us to query the adjacency(topological) information when it is required as demonstrated in Section 4.3.

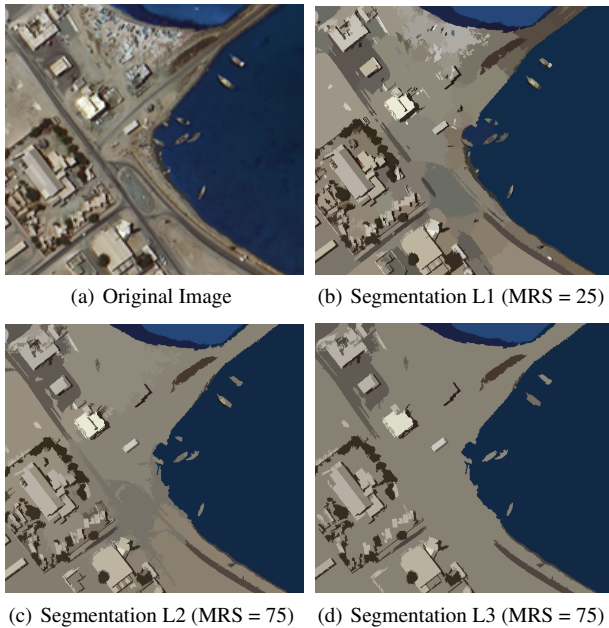


Figure 13: A section of a high-resolution image from WorldView-2 Sensor with a spatial resolution $< 0.5m$ in GSD. Segmentation maps going from fine to coarse details.

5 CONCLUSIONS AND FUTURE WORK

The importance of including topological information in the object model was discussed. Currently, the region descriptors in our object model i.e. image regions as objects includes the spectral signature, texture, and gradient information (Vantaram et al., 2011, Syed et al., 2011). Adding on topological descriptions to the model will enable us to capture the arrangement of objects/regions, allowing the possibility of leveraging the contextual information present in the images.

Two methods to extract and encode topological relationships between image regions were explored: The RCC-8 Model and the CM model. A derivation of the topological predicates of the popular RCC-8 model using the CM model was presented, along with a procedure to query the topology of any two given regions. A simple performance comparison between the pixel-based and the dart-based methods showed that the latter is more efficient.

We find the CM model to be a more elegant approach to extract and encode topological relationships between regions. It parallels the object oriented approach where the label map is decomposed into primitive objects called darts. Once the combinatorial representation has been generated, all references to region are now in terms of darts. Any query about topological relationship between regions is now performed on an array of integers containing the darts rather than the region pixels.

In this paper, a combinatorial map representation and framework to query topology for a single level segmentation was presented. The objective of our current research is to extend this representation to multi-scale segmentation allowing for topological queries across different levels of an hierarchy containing segmentations of multiple scales.

REFERENCES

Alboody, A., Sedes, F. and Inglada, J., 2009. Multi-level topological relations of the spatial reasoning system rcc-8. In: Proceedings of the 2009 First International Conference on Advances in

Databases, Knowledge, and Data Applications, IEEE Computer Society, Washington, DC, USA, pp. 13–21.

Behr, T. and Schneider, M., 2001. Topological relationships of complex points and complex regions. In: In Proceedings of the International Conference on Conceptual Modeling, pp. 56–69.

Blaschke, T., 2009. Object based image analysis for remote sensing. *ISPRS Journal of Photogrammetry and Remote Sensing* 65(1), pp. 2 – 16.

Braquelaire, A. J.-P., 2005. Representing and segmenting 2d images by means of planar maps with discrete embeddings: From model to applications. In: *GbRPR*, pp. 92–121.

Braquelaire, J.-P. and Brun, L., 1998. Image segmentation with topological maps and inter-pixel representation. *Journal of Visual Communication and Image Representation* 9(1), pp. 62 – 79.

Braquelaire, J.-P. and Domenger, J.-P., 1999. Representation of segmented images with discrete geometric maps. *Image and Vision Computing* 17(10), pp. 715 – 735.

Chen, J., Pan, D. and Mao, Z., 2009. Image-object detectable in multiscale analysis on high-resolution remotely sensed imagery. *International Journal of Remote Sensing* 30(14), pp. 3585–3602.

Castilla, G., Hay, G.G. and Ruiz-Gallardo, J.R., 2008. Size-constrained Region Merging (SCRM): An Automated Delineation Tool for Assisted Photointerpretation. *Journal of the American Society for Photogrammetry and Remote* 74(4), pp. 409–420.

Damiand, G., Bertrand, Y. and Fiorio, C., 2004. Topological model for two-dimensional image representation: definition and optimal extraction algorithm. *Computer Vision and Image Understanding* 93(2), pp. 111 – 154.

Dey, V., Zhang, Y. and Zhong, M., 2010. A review on image segmentation techniques with remote sensing perspective. *ISPRS TC VII Symposium XXXVIII*, pp. 31–42.

Egenhofer, M. J., 1991. Reasoning about binary topological relations. In: *SSD*, pp. 143–160.

Hay, G. J. and Castilla, G., 2006. Object-based image analysis: strengths, weaknesses, opportunities and threats (swot). *International Archives of Photogrammetry Remote Sensing and Spatial Information Sciences* 36, pp. 4.

Inglada, J. and Michel, J., 2007. Spatial reasoning and multiscale segmentation for object recognition in hr optical remote sensing images. In: *Geoscience and Remote Sensing Symposium, 2007. IGARSS 2007. IEEE International*, pp. 4798 –4801.

Inglada, J. and Michel, J., 2009. Qualitative spatial reasoning for high-resolution remote sensing image analysis. *Geoscience and Remote Sensing, IEEE Transactions on* 47(2), pp. 599 –612.

Marangoz, A.M., O. M. and Buyuksalih, A., 2004. Object-oriented image analysis and semantic network for extracting the roads and buildings from ikonos pan-sharpened images. *20th ISPRS Congress*.

Randell, D. A., Cui, Z. and Cohn, A. G., 1992. A spatial logic based on regions and connection. In: *Proceedings 3rd International Conference on Knowledge Representation and Reasoning*.

Syed, A. H., Saber, E. and Messinger, D., 2011. Scale-space representation of remote sensing images using an object-oriented approach. Vol. 8053 Number 1, *SPIE*, p. 805308.

Vantaram, S. R., Saber, E. and Messinger, D., 2011. An intensity-gradient-texture guided methodology for spatial segmentation of remotely sensed multi/hyperspectral imagery. In: *ICIP*, pp. 2885–2888.